Journal of Fluids and Structures (1997) **11,** 183–205

A LINEARIZED UNSTEADY MODEL FOR COMPUTING DYNAMICS OF CYLINDRICAL STRUCTURES SUBJECTED TO NONUNIFORM ANNULAR FLOWS AT HIGH REYNOLDS NUMBERS

L. Perotin and S. Granger
Research and Development Division, Electricité de France, 6, Quai Watier 78401 Chatou Cedex, France

(Received 9 August 1995 and in revised form 18 October 1996)

The stability of co-axial cylindrical structures subjected to annular flows has received a lot of attention in the last few years. Configurations of this kind are widely encountered in Pressurized Water Reactor (PWR) components and are therefore of important practical interest. This paper presents a linearized unsteady model for computing the fluid–structure interaction between an axial annular flow and a vibrating structure. This model, implemented into a computer code, MOCCA, deals with an incompressible viscous fluid, flowing at high Reynolds number, in a finite length annular region the cross-section of which may vary continuously with axial position. Both differences and similarities with the model previously developed by Hobson are pointed out. A comparison is also made with experimental data, for a cylinder that is free to oscillate under the action of a nonuniform annular flow.

1. INTRODUCTION

The stability of co-axial cylindrical structures submitted to annular flows has received a great deal of attention in the last few years. Configurations of this kind are widely encountered in Pressurized Water Reactor (PWR) components, and are therefore of important practical interest. The dynamics and stability of a cylinder confined within a duct and submitted to an axial annular flow were investigated in an analytical manner by Hobson (1982) and Spurr & Hobson (1984). The related one-dimensional approaches of Mulcahy, (1988) and Inada & Hayama (1990) ought also to be mentioned. On the other hand, Mateescu and Païdoussis (1985) proposed a different modelling of the same problem based upon potential flow theory. This formulation was extended later by considering dissipative terms (Mateescu and Païdoussis 1987), and, then, by taking into account end effects (de Langre *et al.* 1992). Recently, Mateescu and co-workers have developed two computational methods for solving unsteady flows between oscillating cylinders: (i) a time-integration method based on a finite difference formulation (Mateescu *et al.* 1994), and (ii) a hybrid spectral method (Mateescu *et al.* 1995).

This paper presents a linearized unsteady model for computing the fluid–structure interaction between an axial annular flow and a vibrating structure. This model, implemented into a computer code, MOCCA, deals with an incompressible viscous fluid, flowing *at high Reynolds number,* in a finite length annular region the cross-section of which may vary continuously with axial position. The system under

0889–9746/97/020183 + 23 $25.00/fl960072

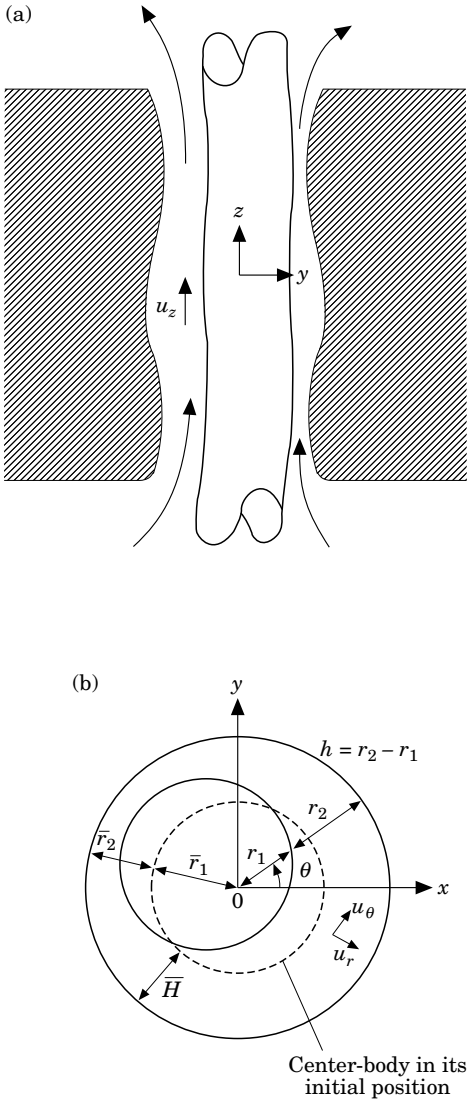

Figure 1. Two co-axial oscillating cylinders submitted to a nonuniform annular flow (to simplify, only the motion of the inner cylinder has been represented in the figure).

consideration is shown in Figure 1 where some of the notations used later on are also defined. In the annular region, the flow is assumed to be governed by the continuity and unsteady Navier-Stokes equations associated with the no flow-through condition and a boundary condition relating turbulent wall-friction to flow velocity. The Method of Integral Relations is then used to integrate the governing partial differential equations along the radial direction, so that (i) the original equations are replaced by a system of equations containing independent variables reduced by one, and (ii) the boundary conditions are naturally taken into account in the integrated equations.

Based on the small amplitude motion assumption and the hypothesis that motion-induced flow perturbations interact only with the mean turbulent flow, the unsteady integrated equations can be linearized and the solution can be sought as the sum of two components: a mean steady flow assuming fixed boundaries and a motion-induced

unsteady flow perturbation. To close the model, two supplementary sets of boundary conditions are supplied at the inlet and outlet of the annular region. They are based on energy conservation considerations. The fluid flow equations are then coupled with the structural motion equations expressed in the modal basis.

In contrast to the methods of Mateescu *et al.* (1994, 1995), this model can deal with turbulent annular flows which are one of the main topics of this paper. The present approach has some similarities but also some significant differences with the axisymmetric two-dimensional Hobson model. They are discussed in detail, on the basis of a theoretical comparative study.

The results obtained with the MOCCA code are finally compared to experimental data and to solutions from the Hobson model, for the flow-induced vibrations of the outer part of an annular passage of variable cross-section, formed by a pair of co-axial cylindrical bodies.

2. GENERAL CONSIDERATIONS

The mass and momentum conservation equations, for an incompressible fluid, can be expressed as

$$\begin{aligned} &\operatorname{div} \boldsymbol{u} = 0 \\ &\frac{\partial \boldsymbol{u}}{\partial t} + \boldsymbol{u} \cdot \nabla \boldsymbol{u} = -\frac{1}{\rho} \nabla p + \frac{1}{\rho} \operatorname{div} \boldsymbol{\tau}, \end{aligned} \tag{1}$$

where $\boldsymbol{u}$ is the flow velocity, p is the pressure, ρ is the fluid density and $\boldsymbol{\tau}$ is the stress tensor field.† To formulate a well-posed problem, an additional constitutive equation relating the stress tensor field to the other flow variables, and initial and wall boundary conditions must be specified. Two cases are usually distinguished.

(i) *Laminar flows*

The stress tensor field is modelled as

$$\boldsymbol{\tau} = \mu(\nabla \mathbf{u} + \nabla \mathbf{u}^{\mathrm{T}}), \tag{2a}$$

where μ is the fluid viscosity. The wall boundary conditions are the no flow-through and the no slip conditions,

$$\boldsymbol{u} \cdot \boldsymbol{n} = \boldsymbol{u}_w \cdot \boldsymbol{n} \qquad \text{and} \qquad \boldsymbol{u} \times \boldsymbol{n} = \boldsymbol{u}_w \times \boldsymbol{n}, \tag{2b}$$

where $\boldsymbol{n}$ denotes the unit outer normal to the fluid at the wall and $\boldsymbol{u}_w$ represents wall velocity.

(ii) *Turbulent flows*

In a turbulent flow, the flow variables, such as velocity and pressure, fluctuate in space and time in an apparently random manner. Each flow variable may therefore be decomposed into an average and a zero mean fluctuating component. To obtain a mathematical model for the mean turbulent flow, the continuity and Navier-Stokes equations are averaged. The resulting equations are identical to equation (1) except that the tensor field, $\boldsymbol{\tau}$, now includes an extra stress, i.e., the Reynolds stress, for which an additional constitutive equation, usually referred to as a "turbulence model", is needed.

† Throughout, vectors are denoted by sloping bold symbols, while tensors by *upright* bold symbols.

In the literature, the most commonly used turbulence models are the algebraic eddy viscosity and $k - \varepsilon$ models. In both cases, the total stress tensor field is expressed as

$$\boldsymbol{\tau} = (\mu + \mu_T)(\nabla \mathbf{u} + \nabla \mathbf{u}^{\mathrm{T}}), \tag{3a}$$

where the eddy viscosity, μ_T, is given by the turbulence model. The wall boundary conditions are also usually different from equation (2b) and have the following general form:

$$\boldsymbol{u} \cdot \boldsymbol{n} = \boldsymbol{u}_w \cdot \boldsymbol{n} \qquad \text{and} \qquad \boldsymbol{\tau} \cdot \boldsymbol{n} = \boldsymbol{\tau}^*(\boldsymbol{u}^*), \qquad \text{with} \qquad \boldsymbol{\tau}^* \cdot \mathbf{n} = 0. \tag{3b}$$

In these equations, the no flow-through condition is naturally retained, but the no slip condition is replaced by a nonlinear equation relating the wall shear stress, $\boldsymbol{\tau}^*$, to the flow velocity field *outside* the boundary layer, $\boldsymbol{u}^*$ (Schlichting 1968; Gunzburger & Nicolaides 1993).

Based on this line of thought, various Computational Fluid Dynamics (CFD) codes suited to solving *fixed* boundary flow problems have been developed, during the last 10 years, in many universities and industrial laboratories. For its part, the Research and Development division of Electricité de France (EDF) has developed a CFD code, N3S (Chabard 1992), which allows the computation of two and three-dimensional turbulent incompressible flows. In this code, the Finite Element Method is used together with a $k - \varepsilon$ turbulence model.

Applied to our problem, this kind of CFD code can yield an estimation of the mean turbulent flow when the structure is *motionless.* The aim of the unsteady linearized model to be described below is to complement such a CFD code in order to enable the determination of the unsteady mean turbulent flow in the presence of *moving walls.*

3. INTEGRATED EQUATIONS FOR MOTION-INDUCED VELOCITY AND PRESSURE FIELDS

3.1. Method of Integral Relations

The Method of Integral Relations was originally formulated by Dorodnitsyn (1956). It is an extension of the method known, in fluid mechanics, as the Kármán-Pohlhausen technique. The Method of Integral Relation has been presented in detail by Holt (1984) and is referred to as the Integral Method in Zwillinger (1989). Since the work of Dorodnitsyn, this technique has been subsequently applied to a wide variety of current problems in fluid dynamics, and, in particular, to the solution of incompressible laminar boundary layer equations. The basic idea of this method is to integrate the governing partial differential equations, with respect to one of the independent variables. The original equations can thus be replaced by a system of equations containing independent variables reduced by one. To this end, the unknowns are linearly expanded using arbitrary interpolation functions of the integration variable. Such functions are chosen according to the problem in question (polynomials, trigonometric expressions, etc.). Solving the system then reduces to identifying the coefficients of the above-mentioned expansion. The integration domain may be divided into several subdomains. The original partial differential equations must then be multiplied by as many given independent functions as subdomains, before being integrated. This method allows us to take into account the boundary conditions in the integrated formulation, as well as possible boundary motions. This is the reason why this technique is often used in free-boundary problems.

When applied to the problem depicted in Figure 1, the Method of Integral Relations

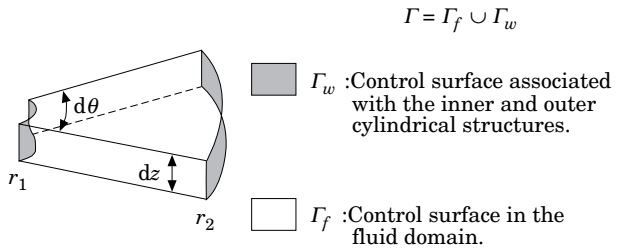

Figure 2. Control volume Ω used in the Method of Integral Relations.

is equivalent to integrating equations (1) over the control volume Ω shown in Figure 2; Γ_f denotes the control surface in the fluid domain, and Γ_w denotes the control surface associated with the inner and outer cylindrical structures. Gauss' divergence theorem and boundary conditions (3b) then yield:

Mass conservation

$$\int_{\Gamma_f(t)} \boldsymbol{u} \cdot \boldsymbol{n} \, d\gamma = - \int_{\Gamma_w(t)} \boldsymbol{u}_w \cdot \boldsymbol{n} \, d\gamma. \tag{4}$$

Linear momentum conservation

$$\int_{\Omega(t)} \frac{\partial \boldsymbol{u}}{\partial t} d\omega + \int_{\Gamma_f(t)} \boldsymbol{u}(\boldsymbol{u} \cdot \boldsymbol{n}) \, d\gamma + \int_{\Gamma_f \cup \Gamma_w(t)} \frac{p}{\rho} \boldsymbol{n} \, d\gamma - \int_{\Gamma_f(t)} \frac{1}{\rho} \boldsymbol{\tau} \cdot \boldsymbol{n} \, d\gamma$$
$$= \int_{\Gamma_w(t)} \frac{1}{\rho} \boldsymbol{\tau}^* \, d\gamma - \int_{\Gamma_w(t)} \boldsymbol{u}_w (\boldsymbol{u}_w \cdot \boldsymbol{n}) \, d\gamma. \tag{5}$$

In cylindrical coordinates, equation (4) becomes

$$\frac{\partial}{\partial t}\left[\int_{r_1}^{r_2} r \, dr\right] + \frac{\partial}{\partial \theta}\left[\int_{r_1}^{r_2} u_\theta \, dr\right] + \frac{\partial}{\partial z}\left[\int_{r_1}^{r_2} r u_z \, dr\right] = 0. \tag{6}$$

In the same way, equations (5) yield the following two integral relations in the z and θ directions respectively:

$$\frac{\partial}{\partial t}\left[\int_{r_1}^{r_2} r u_z \, dr\right] + \frac{\partial}{\partial \theta}\left[\int_{r_1}^{r_2} u_\theta u_z \, dr\right] + \frac{\partial}{\partial z}\left[\int_{r_1}^{r_2} r u_z^2 \, dr\right]$$
$$+ \frac{1}{\rho}\frac{\partial}{\partial z}\left[\int_{r_1}^{r_2} p r \, dr\right] + \frac{1}{\rho} r_1 \frac{\partial r_1}{\partial z} p\big|_{r_1} - \frac{1}{\rho} r_2 \frac{\partial r_2}{\partial z} p\big|_{r_2}$$
$$= \frac{1}{\rho} r_2 \tau_z^*\big|_{r_2} + \frac{1}{\rho} r_1 \tau_z^*\big|_{r_1} + \frac{1}{\rho}\frac{\partial}{\partial \theta}\left[\int_{r_1}^{r_2} \tau_{\theta z} \, dr\right] + \frac{1}{\rho}\frac{\partial}{\partial z}\left[\int_{r_1}^{r_2} r \tau_{zz} \, dr\right]; \tag{7}$$

$$\frac{\partial}{\partial t}\left[\int_{r_1}^{r_2} r u_\theta \, dr\right] + \frac{\partial}{\partial \theta}\left[\int_{r_1}^{r_2} u_\theta^2 \, dr\right] + \frac{\partial}{\partial z}\left[\int_{r_1}^{r_2} r u_\theta u_z \, dr\right]$$
$$+ \int_{r_1}^{r_2} u_r u_\theta \, dr + \frac{\partial}{\partial \theta}\left[\int_{r_1}^{r_2} \frac{p}{\rho} dr\right] + \frac{\partial r_1}{\partial \theta}\frac{p}{\rho}\bigg|_{r_1} - \frac{\partial r_2}{\partial \theta}\frac{p}{\rho}\bigg|_{r_2}$$
$$= \frac{1}{\rho} r_2 \tau_\theta^*\big|_{r_2} + \frac{1}{\rho} r_1 \tau_\theta^*\big|_{r_1} + \frac{1}{\rho}\frac{\partial}{\partial \theta}\left[\int_{r_1}^{r_2} \tau_{\theta\theta} \, dr\right]$$
$$+ \frac{1}{\rho}\frac{\partial}{\partial z}\left[\int_{r_1}^{r_2} r \tau_{\theta z} \, dr\right] + \frac{1}{\rho}\int_{r_1}^{r_2} \tau_{r\theta} \, dr. \tag{8}$$

The radial component of equations (5) does not appear explicitly in the present model, similarly to Prandtl's boundary layer equations. This point is discussed in Section 3.2. Proceeding as usual within the framework of the Method of Integral Relations, a solution to equations (6–8) can be obtained by approximating the unknown velocity and pressure fields $(\boldsymbol{u}, p)$ by a suitable expansion in terms of interpolation functions. This expansion is presented in the following section.

3.2. Perturbation Analysis; Velocity and Pressure Distributions Along the Radial Direction.

As we shall consider the *linear* stability of the coupled fluid–structure system, vibratory amplitudes can therefore be assumed to be small relative to the mean annular gaps. As a consequence, the motion-induced velocity and pressure perturbations are also supposed to be small, compared to the mean turbulent flow velocity and pressure fields in the absence of structural motion. Moreover, we also assume that the motion-induced flow perturbations interact only with the mean turbulent flow. Consequently, we can seek the solution $(\boldsymbol{u}, p)$ of equations (6–8) in the following form:

$$\begin{aligned} \boldsymbol{u}(r, \theta, z, t) &= \bar{\boldsymbol{U}}(r, \theta, z) + \tilde{\boldsymbol{u}}(r, \theta, z, t), \\ p(r, \theta, z, t) &= \bar{P}(r, \theta, z) + \tilde{p}(r, \theta, z, t), \end{aligned} \tag{9}$$

with $|\tilde{\boldsymbol{u}}| \ll |\bar{\boldsymbol{U}}|$ and $|\tilde{p}| \ll |\bar{P}|$. In this expression, $(\tilde{\boldsymbol{u}}, \tilde{p})$ represent the motion-induced velocity and pressure peturbations, while $(\bar{\boldsymbol{U}}, \bar{P})$ denote mean turbulent flow velocity and pressure fields associated to a fixed fluid domain which has still to be determined.

To proceed further and, in particular, to be able to complete the determination of the fixed fluid domain associated to the mean turbulent flow, we transform the time-varying physical domain, $\mathscr{D}(t) = [r_1(t), r_2(t)] \times [0, 2\pi] \times [0, L]$ into the fixed computational domain, $\mathscr{D}_0 = [-1, +1] \times [0, 2\pi] \times [0, L]$. This is achieved by defining the variable, η, as

$$r = r_0 + \eta \frac{h}{2} \quad \text{with} \quad \begin{cases} r_0 = \dfrac{r_1 + r_2}{2}, \\ h = r_2 - r_1; \end{cases} \tag{10}$$

η lies between -1 and $+1$ when r varies between r_1 and r_2. Consequently, substituting equation (10) into equations (6–8) yields, in terms of variables (η, θ, z), an equivalent set of equations associated with the fixed computational domain $\mathscr{D}_0$. For example equation (6) becomes:

$$\frac{\partial (r_0 h)}{\partial t} + \frac{\partial}{\partial \theta}\left(\frac{h}{2}\int_{-1}^{+1} u_\theta \, \mathrm{d}\eta\right) + \frac{\partial}{\partial z}\left(\frac{h}{2}\int_{-1}^{+1} \left(r_0 + \eta \frac{h}{2}\right) u_z \, \mathrm{d}\eta\right) = 0, \tag{11}$$

with similar expressions for the linear momentum conservation equations in the z and θ directions.

Taking the expansion defined by equation (9) into account, this new set of conservation equations can be further decomposed by a perturbation analysis into: (i) a set of first order conservation equations involving only the mean turbulent flow variables $(\bar{\boldsymbol{U}}, \bar{P})$, and (ii) a set of second order conservation equations characterizing the motion-induced velocity and pressure fields $(\tilde{\boldsymbol{u}}, \tilde{p})$. Equation (11) thus yields:

First order (*steady part*)

$$\frac{\partial}{\partial\theta}\left[\frac{\bar{H}}{2}\int_{-1}^{+1}\bar{U}_\theta\,\mathrm{d}\eta\right]+\frac{\partial}{\partial z}\left[\frac{\bar{H}}{2}\int_{-1}^{+1}\left(\bar{R}_0+\eta\frac{\bar{H}}{2}\right)\bar{U}_z\,\mathrm{d}\eta\right]=0. \tag{12}$$

Second order (*unsteady part*)

$$\begin{aligned}\bar{R}_0\frac{\partial\tilde{h}}{\partial t}+\bar{H}\frac{\partial\tilde{r}_0}{\partial t}+\frac{\bar{H}}{2}\frac{\partial}{\partial\theta}\left[\int_{-1}^{+1}\tilde{u}_\theta\,\mathrm{d}\eta\right]\\ +\frac{\partial}{\partial z}\left[\frac{\bar{H}}{2}\int_{-1}^{+1}\left(\tilde{r}_0+\eta\frac{\tilde{h}}{2}\right)\bar{U}_z\,\mathrm{d}\eta+\frac{\bar{H}}{2}\int_{-1}^{+1}\left(\bar{R}_0+\eta\frac{\bar{H}}{2}\right)\tilde{u}_z\,\mathrm{d}\eta\right]\\ +\frac{\partial}{\partial\theta}\left[\frac{\tilde{h}}{2}\int_{-1}^{+1}\bar{U}_\theta\,\mathrm{d}\eta\right]+\frac{\partial}{\partial z}\left[\frac{\tilde{h}}{2}\int_{-1}^{+1}\left(\bar{R}_0+\eta\frac{\bar{H}}{2}\right)\bar{U}_z\,\mathrm{d}\eta\right]=0.\end{aligned} \tag{13}$$

In these equations, $\bar{R}_0$, $\tilde{r}_0$, $\bar{H}$ and $\tilde{h}$ are defined as

$$\begin{aligned}r_0(\theta, z, t)&=\bar{R}_0(z)+\tilde{r}_0(\theta, z, t),\\ h(\theta, z, t)&=\bar{H}(z)+\tilde{h}(\theta, z, t).\end{aligned} \tag{14}$$

Similar expressions can also be derived for the linear momentum conservation equations in the z and θ directions.

The first-order equations show that the fixed fluid problem to which the mean turbulent flow velocity and pressure fields ($\bar{\boldsymbol{U}}$, $\bar{P}$) are associated, is simply the annular region when the structure is initially at rest, i.e., $\mathscr{D}(0)=[\bar{r}_1, \bar{r}_2]\times[0, 2\pi]\times[0, L]$. As noted in Section 2, the mean turbulent flow in $\mathscr{D}(0)$ can be computed once and for all by using a CFD code such as N3S. These data can then be used in the second order integral relations to calculate the motion-induced flow variables ($\tilde{\boldsymbol{u}}$, $\tilde{p}$) [see equation (13)]. Moreover, as we consider narrow annular gaps, the expressions for $\tilde{\boldsymbol{u}}$ and $\tilde{p}$ can be made more precise as follows.

(i) Because the annular clearance is small, the radial component of the motion-induced velocity is quickly redistributed in the θ and z directions, through the mass conservation equation, as soon as the fluid gets away from the moving structure. In the integral relations, the influence of $\tilde{u}_r$ can thus be neglected with respect to that of $\tilde{u}_\theta$ and $\tilde{u}_z$. In particular, the integral from r_1 to r_2 of $\tilde{u}_r$ will be small compared to the integral from r_1 to r_2 of $\tilde{u}_\theta$ and $\tilde{u}_z$, even though $\tilde{u}_r$ is naturally predominant near the moving walls. In the present case, this simplification constitutes a supplementary advantage of the Method of Integral Relations. This also explains why the radial component of the linear momentum conservation equation is not used in the MOCCA formulation.

(ii) The radial variation of each velocity and pressure perturbation is assumed to be identical to that of its first order counterpart. Similarly to the previous hypothesis, this assumption is also based on the smallness of the annular gap which induces a weaker propagation of the disturbances in the radial direction. However, as the geometry is axisymmetric when the cylinders are in their equilibrium position, $\bar{U}_\theta$ is equal to zero. The $\tilde{u}_\theta$ distribution in the r direction is therefore supposed to be identical to the $\tilde{u}_z$ and $\bar{U}_z$ profile. For smoothly varying annular gaps, this hypothesis amounts to leaving the radial distribution of the flow velocity component tangential to the walls, i.e. $\boldsymbol{u}\times\boldsymbol{n}$, unchanged with regard to the perturbations. From these two assumptions, the

following refined expansion can be specified for the flow variables $(\boldsymbol{u}, p)$:

$$\begin{aligned} u_r(\eta, \theta, z, t) &= [\bar{U}_r^+(z)]\phi_r(\eta, z), \\ u_\theta(\eta, \theta, z, t) &= [\tilde{u}_\theta^+(\theta, z, t)]\phi_z(\eta, z), \\ u_z(\eta, \theta, z, t) &= [\bar{U}_z^+(z) + \tilde{u}_z^+(\theta, z, t)]\phi_z(\eta, z), \\ p(\eta, \theta, z, t) &= [\bar{P}^+(z) + \tilde{p}^+(\theta, z, t)]\phi_p(\eta, z), \end{aligned} \tag{15}$$

where the ϕs are the velocity and pressure distributions; they assume values between -1 and $+1$. $\bar{U}_r^+$, $\bar{U}_z^+$ and $\bar{P}^+$ are the extrema of $\bar{U}_r$, $\bar{U}_z$ and $\bar{P}$ in the r direction. It should be noted that ϕ_r, ϕ_z and ϕ_p are deduced from the mean turbulent flow computation. In particular, because of the narrowness of the annular gap, it happens that $\phi_p(\eta, z) \approx 1$ in practical applications.

Taking equation (15) into account, the second-order integral relation expressing mass conservation [equation (13)] can be rewritten as

$$\begin{aligned} &\bar{H}\frac{\partial \tilde{r}_0}{\partial t} + \bar{R}_0\frac{\partial \tilde{h}}{\partial t} + \frac{\bar{H}}{2}\left[\int_{-1}^{+1}\phi_z\,\mathrm{d}\eta\right]\frac{\partial \tilde{u}_\theta^+}{\partial \theta} \\ &\quad + \frac{\partial}{\partial z}\left[\frac{\bar{U}_z^+}{2}\int_{-1}^{+1}\left(\bar{H}\left(\tilde{r}_0 + \eta\frac{\tilde{h}}{2}\right) + \tilde{h}\left(\bar{R}_0 + \eta\frac{\bar{H}}{2}\right)\right)\phi_z\,\mathrm{d}\eta\right] \\ &\quad + \frac{\partial}{\partial z}\left[\frac{\bar{H}}{2}\int_{-1}^{+1}\left(\bar{R}_0 + \eta\frac{\bar{H}}{2}\right)\phi_z\,\mathrm{d}\eta\right]\tilde{u}_z^+ \\ &\quad + \left[\frac{\bar{H}}{2}\int_{-1}^{+1}\left(\bar{R}_0 + \eta\frac{\bar{H}}{2}\right)\phi_z\,\mathrm{d}\eta\right]\frac{\partial \tilde{u}_z^+}{\partial z} = 0. \end{aligned} \tag{16}$$

Similar expressions for the integral relations representing the linear momentum conservation in the z and θ directions can be obtained in the same manner. They are given in Appendix A. These equations give the viscous and turbulent (Reynolds) stresses. Constitutive equations relating the stress tensor field to flow velocity will now be specified, in order to obtain a closed system of three partial differential equations, with respect to θ, z and t. This is the purpose of the next section.

4. VISCOUS AND TURBULENT STRESS MODELLING IN UNSTEADY EQUATIONS

To proceed in the same spirit as the analysis presented in Section 3.2, the most logical approach for fluid stress modelling would have been to apply a perturbation technique, in order to develop a quasi-steady model of the dissipative terms, on the basis of the turbulence model implemented in the CFD code used to determine mean turbulent velocity and pressure fields. However, a simplified approach has been retained in the present model.

This approach consists of assuming that the main part of dissipation is located near the walls. Viscous and turbulent stresses inside the fluid domain are thus neglected, *in the second order linear momentum conservation equations,* and frictional shear stresses on walls are modeled *via* a quasi-steady expansion of the following usual skin friction law for pipe-flow (Idelchik 1986):

$$\boldsymbol{\tau}^* = -\tfrac{1}{2}\rho C_F\,|\boldsymbol{u}|\,\boldsymbol{u}. \tag{17}$$

In this expression, $\boldsymbol{u}$ is the flow velocity outside the boundary layer and C_F is the friction coefficient on walls, which depends on Reynolds number,

$$\mathrm{Re} = 2\bar{H}\,|\boldsymbol{u}|/\nu. \tag{18}$$

Expanding C_F into a steady and an unsteady part, equation (17) yields

$$\begin{aligned} &\bar{\tau}^*_\theta = 0, \qquad \tilde{\tau}^*_\theta = -\tfrac{1}{2}\rho \bar{C}_F\, |\bar{\boldsymbol{U}}| \tilde{u}_\theta, \\ &\bar{\tau}^*_z = -\tfrac{1}{2}\rho \bar{C}_F\, |\bar{\boldsymbol{U}}|\, \bar{U}_z, \qquad \tilde{\tau}^*_z = -\tfrac{1}{2}\rho [\bar{C}_F \tilde{u} \bar{U}_z + \bar{C}_F\, |\bar{\boldsymbol{U}}|\, \tilde{u}_z + \tilde{C}_F\, |\bar{\boldsymbol{U}}|\, \bar{U}_z], \end{aligned} \tag{19}$$

where $\bar{C}_F$ represents the friction coefficient resulting from the mean turbulent flow and $\tilde{C}_F$ is the part of the friction coefficient due to the motion-induced flow perturbation; $|\bar{\mathbf{U}}|$ and $\tilde{u}$ are given by

$$|\bar{\boldsymbol{U}}| = \sqrt{\bar{U}_r^2 + \bar{U}_z^2} \quad \text{and} \quad \tilde{u} = \frac{\bar{U}_z}{|\bar{\boldsymbol{U}}|} \tilde{u}_z. \tag{20}$$

Let $\bar{C}_F$ be expressed as (Idelchik 1986)

$$\bar{C}_F = C_{F_0}\, \overline{\mathrm{Re}}^m, \tag{21}$$

with $m = m\,(\overline{\mathrm{Re}})$ and $C_{F_0} = C_{F_0}(\overline{\mathrm{Re}})$; $\tilde{C}_F$ can be deduced from the expression for $\bar{C}_F$ by making a quasi-steady approximation of C_F. We thus obtain

$$\tilde{C}_F = m C_{F_0}\, \widetilde{\mathrm{Re}}\, \overline{\mathrm{Re}}^{m-1} = m \bar{C}_F [\bar{U}_z / |\bar{\boldsymbol{U}}|^2] \tilde{u}_z. \tag{22}$$

The exact variations of m and $\bar{C}_F$ with Reynolds number, $\overline{\mathrm{Re}}$, are given explicitly in Appendix B. They are derived from Blasius' formula and the generalized Kármán-Nikuradze law (Prandtl 1936; Idelchik 1986).

5. SOLUTION OF THE PARTIAL DIFFERENTIAL EQUATIONS

Taking equations (20) and (22) into account, and inserting equation (19) into equations (16), (A1) and (A2) (Appendix A), a closed system of three partial differential equations, with respect to θ, z and t, can be obtained. In this section, it is first transformed into an equivalent system of three ordinary differential equations with respect to the space variable, z. Three inlet-outlet boundary conditions are then imposed, allowing the unsteady fluid problem to be solved.

5.1. Derivation of the Equivalent System of Ordinary Differential Equations

As the system of partial differential equations obtained at the end of Section 3 is linear, we can seek the solution in the Laplace domain, in order to replace derivatives with respect to time by algebraic expressions with respect to the Laplace variable, s. Then, we consider that one of the coaxial cylinders is motionless and that the other one vibrates according to a rigid body or beam-like mode shape associated with a given mode of vibration. Furthermore, as the geometry is axisymetric when the cylinders are in their equilibrium position, it is not restrictive to consider, in the following development, that motion takes place in the x direction. We can therefore set in the Laplace domain,

$$\tilde{h}(\theta, z, s) = h^+(z) \cos\theta q(s), \qquad \tilde{r}_0(\theta, z, s) = r_0^+(z) \cos\theta q(s), \tag{23}$$

where h^+ and r_0^+ are deduced from the mode shape of the vibrating structure and $q(s)$ is the modal amplitude of vibration. Consequently, due to the particular form of the partial differential equations derived in Section 3, the form of the unsteady velocity and pressure fields can be specified further as follows:

$$\begin{aligned} &\tilde{u}_\theta^+(\theta, z, s) = u_0^+(z, s) \sin\theta q(s), \qquad \tilde{u}_z^+(\theta, z, s) = u_z^+(z, s) \cos\theta q(s); \\ &\tilde{p}^+(\theta, z, s) = p^+(z, s) \cos\theta q(s). \end{aligned} \tag{24}$$

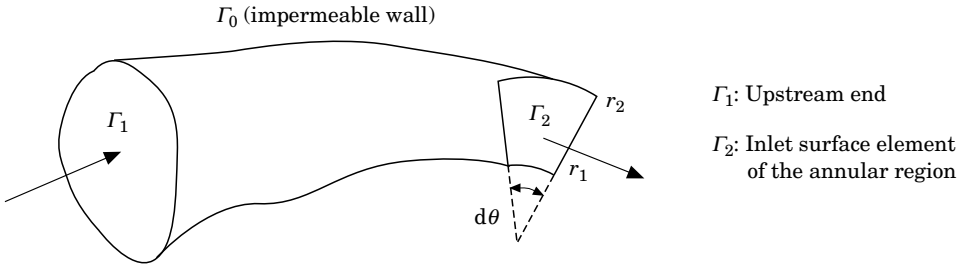

Figure 3. Control volume (consisting of a streamtube) for the inlet boundary condition.

Substituting equation (24) into equations (16), (A1) and (A2) (see Appendix A) provides, in the Laplace domain, the following set of ordinary differential equations, along the z direction:

$$\frac{\partial Y}{\partial z} + AY + B = 0, \qquad Y = (u_\theta^+, u_z^+, p^+)^{\mathrm{T}}, \tag{25}$$

where A is a 3×3 complex matrix which depends only on the mean turbulent flow variables and B is a complex vector which depends on both mean turbulent flow variables and particular mode shape. A and B also depend on the Laplace variable, s, and implicitly on z.

Given an appropriate set of three inlet-outlet boundary conditions, equation (25) can be solved. A fully implicit first-order finite difference method is used.

5.2. Inlet-Outlet Boundary Conditions

The three inlet–outlet boundary conditions necessary to solve equation (25) are derived as follows:

(i) The first two boundary conditions are obtained from the conservation of the kinetic energy of the fluid within two control volumes located outside the annular region. These control volumes are two streamtubes, as depicted in Figures 3 and 4, which extend respectively from the upstream end up to the inlet of the annular passage and from the outlet of the annular passage up to the downstream end.

In these control volumes, only a loose fluid–structure coupling can take place. We can therefore neglect the *direct* mechanical energy exchanges between fluid and structure and apply the kinetic energy conservation equation in its steady form; this amounts to disregard the contribution of the production (unsteady) terms with respect to that of the convection terms. Strictly speaking, this simplification is justified only when there is no motion outside the annular region, as in the configuration to be presented in Section 8. Otherwise, for configurations as depicted in Figure 1, the present formulation has to be corrected for added-mass effects outside the annular

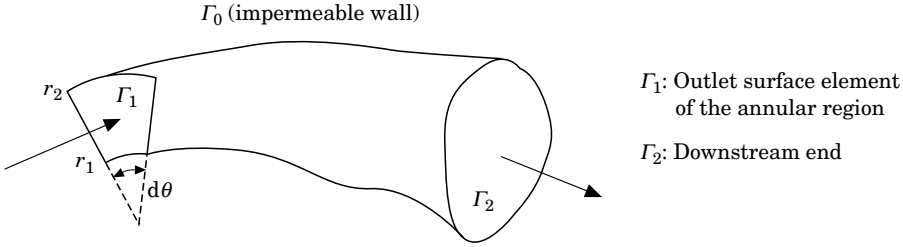

Figure 4. Control volume (consisting of a streamtube) for the outlet boundary condition.

region. Within the annular clearance, where even a small amplitude structural movement can have a great influence on the flow due to the narrowness of the gap, this simplification is obviously no longer applicable.

Denoting by Ω the control volume and Γ the associated control surface, the general steady formulation of the kinetic energy conservation equation can be written as (Richardson 1989)

$$\int_{\Gamma} \tfrac{1}{2}\rho u^2 \boldsymbol{u}\cdot\boldsymbol{n}\,\mathrm{d}\gamma = -\int_{\Gamma} p\boldsymbol{u}\cdot\boldsymbol{n}\,\mathrm{d}\gamma + \int_{\Gamma} \boldsymbol{u}\cdot(\boldsymbol{\tau}\cdot\boldsymbol{n})\,\mathrm{d}\gamma. \tag{26}$$

In this equation, the second term on the right-hand side represents the work done by shear forces per unit time. It takes into account singular and regular friction losses inside the control volume Ω. When Ω is a streamtube, this term is usually modelled as a part of the flux of kinetic energy out through the inlet or outlet surface, i.e. Γ_1 or Γ_2 in Figure 3. Equation (26) then becomes

$$\int_{\Gamma_1} (p + \tfrac{1}{2}\rho u^2)\boldsymbol{u}\cdot\boldsymbol{n}\,\mathrm{d}\gamma = \int_{\Gamma_2} (p + \tfrac{1}{2}\rho u^2)\boldsymbol{u}\cdot\boldsymbol{n}\,\mathrm{d}\gamma + C_{d_i}\int_{\Gamma_i} \tfrac{1}{2}\rho u^2 \boldsymbol{u}\cdot\boldsymbol{n}\,\mathrm{d}\gamma, \tag{27}$$

with

$$C_{d_i} = \left[\int_{\Gamma} \boldsymbol{u}\cdot(\boldsymbol{\tau}\cdot\boldsymbol{n})\,\mathrm{d}\gamma\right] \Big/ \left[\int_{\Gamma_i} \tfrac{1}{2}\rho u^2 \boldsymbol{u}\cdot\boldsymbol{n}\,\mathrm{d}\gamma\right], \qquad i = 1 \text{ or } 2.$$

At second order, the following two equations can thus be obtained, for the two control volumes defined above:

$$\int_{-1}^{+1} [\tilde{p} + \rho(1 + \bar{C}_{D\,\mathrm{input}})\bar{U}_z\tilde{u}_z + \tfrac{1}{2}\rho\tilde{C}_{D\,\mathrm{input}}|\bar{\boldsymbol{U}}|^2]\bar{U}_z\left(\bar{R}_0 + \eta\frac{\bar{H}}{2}\right)\mathrm{d}\eta = 0 \qquad \text{for } z = 0; \tag{28}$$

$$\int_{-1}^{+1} [\tilde{p} + \rho(1 - \bar{C}_{D\,\mathrm{output}})\bar{U}_z\tilde{u}_z - \tfrac{1}{2}\rho\tilde{C}_{D\,\mathrm{output}}|\bar{\boldsymbol{U}}|^2]\bar{U}_z\left(\bar{R}_0 + \eta\frac{\bar{H}}{2}\right)\mathrm{d}\eta = 0 \qquad \text{for } z = L. \tag{29}$$

In these expressions, $\bar{C}_{D\,\mathrm{input}}$ and $\bar{C}_{D\,\mathrm{input}}$ are the steady parts of the singular loss coefficients at the inlet and outlet of the annular region. They take into account the steady shape of wall separations induced at the inlet and outlet by sudden variations in the geometry. They can be obtained from data of the literature (Idelchik 1986) but can also be estimated by a CFD code. $\tilde{C}_{D\,\mathrm{input}}$ and $\tilde{C}_{D\,\mathrm{output}}$ represent the unsteady parts of the singular loss coefficients. They take into account the disturbances induced on wall separations by structural motion and depend on both θ and s; $\tilde{C}_{D\,\mathrm{input}}$ and $\tilde{C}_{D\,\mathrm{output}}$ can be modelled via a quasi-steady expansion involving steady singular loss coefficients which can be obtained from CFD computations. This point is best illustrated by an example and is considered in Section 8.3.

(ii) The third boundary condition is obtained by assuming that the flow is sufficiently regular upstream of the annular passage so that the circumferential component of the flow velocity at the inlet is equal to zero,

$$\tilde{u}_\theta = 0 \qquad \text{for } z = 0. \tag{30}$$

Taking these three boundary conditions into account, equation (25) can be solved, for any given basic structural motion. As the present model is linear, unsteady fluid problems involving several modes of vibration, or movement of both the inner and outer cylinders, can be solved in a similar way by using the principle of superposition.

6. FLUID–STRUCTURE COUPLING

Fluidelastic forces exerted on structures consist of pressure terms acting normal to the walls and frictional terms acting parallel to them. In the model presented in this paper, the vibrating system can equally be the centre-body or the outer structure, and motion can similarly be characterized by one or several modes of vibration, in the x and y directions (see Figure 1). However, to simplify the following presentation, we shall assume that the outer cylindrical body is at rest and that the inner cylinder is vibrating according to N normal modes in the x direction. The general problem can be handled in the very same way although the analytical expressions are more complicated in this case.

In the Laplace domain, the motion of the inner and outer cylinders can therefore be expressed in the form

$$\tilde{r}_1(\theta, z, s) = \sum_{i=1}^{N} r_{1i}^{+}(z)\cos(\theta)q_i(s), \qquad \tilde{r}_2(\theta, z, s) = 0, \tag{31}$$

where $q_i(s)$ represents the ith modal amplitude of vibration and $r_{1i}^{+}(z)$ is the mode shape associated with the ith normal mode of the centre-body.

The motion-induced velocity and pressure fields can thus be determined from equation (24):

$$\begin{aligned}
\tilde{u}_{\theta}^{+}(\theta, z, s) &= \sum_{i=1}^{N} u_{\theta_i}^{+}(z, s)\sin(\theta)q_i(s),\\
\tilde{u}_{z}^{+}(\theta, z, s) &= \sum_{i=1}^{N} u_{z_i}^{+}(z, s)\cos(\theta)q_i(s),\\
\tilde{p}(\theta, z, s) &= \sum_{i=1}^{N} p_i^{+}(z, s)\cos(\theta)q_i(s).
\end{aligned} \tag{32}$$

In this expression, $u_{\theta i}^{+}$, u_{zi}^{+} and p_i^{+} are deduced from the solution of the fluid problem associated with the basic motion:

$$\begin{aligned}
\tilde{h}_i(\theta, z, s) &= \sum_{i=1}^{N} -r_{1i}^{+}(z)\cos(\theta)q_i(s),\\
\tilde{r}_{oi}(\theta, z, s) &= \sum_{i=1}^{N} \tfrac{1}{2}r_{1i}^{+}(z)\cos(\theta)q_i(s).
\end{aligned} \tag{33}$$

Taking equation (19) into account, the generalized fluidelastic force associated with the jth normal mode, Q_j, can finally be expressed as

$$Q_j(s) = \sum_{i=1}^{N} B_{ij}(s)q_i(s), \tag{34}$$

with

$$B_{ij}(s) = -\pi\bar{r}_1 \int_0^L [p_i^{+}\phi_p + \tfrac{1}{2}\rho\bar{C}_F\,|\bar{\boldsymbol{U}}|\,u_{\theta_i}^{+}\phi_z]_{\eta=-1}r_{1j}^{+}\,\mathrm{d}z.$$

B_{ij} denotes the generalized fluidelastic force associated with the jth mode and induced by a unitary displacement of the ith mode. In matrix form, $[B]$ can be viewed as the transfer-function matrix relating the modal responses to the generalized fluidelastic forces. For each mode of vibration, the modal mass M_i^{st}, the modal damping C_i^{st}, and

the modal stiffness K_i^{st}, of the structure in still air are supposed to be known. Introducing

$$M_{ij} = m_i^{st}\delta_{ij}, \quad C_{ij} = C_i^{st}\delta_{ij}, \quad K_{ij} = K_i^{st}\delta_{ij}, \qquad \text{where } \delta_{ij} = \begin{cases} 1 & \text{for } i = j, \\ 0 & \text{for } i \neq j. \end{cases} \tag{35}$$

The coupled fluid–structure system can thus be characterized, in matrix form, by the following equation:

$$[[M]s^2 + [C]s + [K] - [B(s)]]\begin{Bmatrix} q_1 \\ \vdots \\ q_N \end{Bmatrix} = 0, \tag{36}$$

where it should be noted that $[B]$ also depends on flow velocity. *For a given flow velocity*, the solution of this generalized eigenvalue problem leads to the natural circular frequencies ω_i, $i = 1, N$, and the damping coefficients ζ_i, $i = 1, N$, of the coupled fluid–structure system through the usual relation:

$$s_i = (-\xi_i + j\sqrt{1 - \zeta_i^2})\omega_i, \tag{37}$$

where s_i is the ith eigenvalue given by equation (36). The stability of the ith mode of vibration is deduced from the damping coefficient as follows: if $\zeta_i > 0$, the mode is stable, if $\zeta_i = 0$, the instability threshold has been reached, if $\zeta_i < 0$, the mode is unstable.

7. THEORETICAL COMPARISON WITH HOBSON'S MODEL

The pioneering work of Hobson contains a lot of valuable ideas which provide many insights into the physics of the phenomena. When we first attacked the problem of the dynamics and stability of co-axial cylinders subject to annular flow, the study of Hobson's model (Hobson 1982) was of a great help to us. However, we also felt the need to clarify the link between the mathematical formulation of this model and the basic conservation equations of fluid mechanics. This exercise enabled us to bring out the hypotheses which sustain Hobson's model, including the implicit ones. Some of these assumptions seemed too restrictive to us for our practical applications. Furthermore, it also appeared that Hobson's model is not closed, as it involves some parameters which have to be estimated experimentally for each configuration studied. Keeping in mind the most basic ideas of Hobson's modelling, we then developed the new model presented in this paper in order to get rid of these difficulties.

The MOCCA formulation can therefore be considered as a generalization of Hobson's model. The most important differences between the MOCCA formulation and Hobson's model are presented below.

(i) Hobson's model assumes that the outer cylinder consists of a series of constant diameter pipes separated by sudden expansions or contractions, the centre-body being of constant diameter. At the junctions of the annular sections where the flow area changes, inter-element compatibility conditions have to be specified. They are obtained from quasi-steady approximations of the mass and kinetic energy conservation equations which involve loss or pressure recovery coefficients. As discussed in Section 5.2, the use of such a quasi-steady modelling within the time-varying annular region is highly questionable. This procedure has not been retained in the MOCCA formulation, which handles naturally the axial variation of the annular section without requiring its approximation by piecewise constant functions.

(ii) The equations used by Hobson as a starting point of his model can be obtained by integrating equations (1) from r_1 to r_2. This is not tantamount to integrating equations (1) over the control volume shown in Figure 2, as it is done in the present model. The latter procedure has the advantage of satisfying exactly mass conservation in any case. This does not hold true for Hobson's method except if the annular section does not vary axially. In particular, in the practical configuration to be presented in Section 8, the axial flow velocity is underestimated by 20% with Hobson's model, downstream of the diffuser.

(iii) Hobson implicitly assumes that the pressure and velocity profiles along the r direction are constant and equal to 1. He also considers, in each constant diameter pipe, the following simplified mean turbulent velocity and pressure fields:

$$\bar{U}_r(r, z) = 0, \qquad \bar{U}_z(r, z) = \text{const} = \bar{U},$$

and

$$\bar{P}(r, z) = \bar{P}(z) \quad \text{with} \quad \mathrm{d}\bar{P}/\mathrm{d}z = \text{const} = -\rho \bar{C}_F(\bar{U}^2/\bar{H})$$

Although this approximation is justified for annular passages of constant section, it may be inaccurate in the case of nonuniform annular flows. The use of a CFD code to compute the mean turbulent flow overcomes this problem.

(iv) Hobson also introduced regular and singular loss coefficients in his model. He assumed that $\bar{C}_{D\,\text{input}}$ and $\tilde{C}_{D\,\text{input}}$ are equal to zero, but took $\bar{C}_F$, $\tilde{C}_F$, $\bar{C}_{D\,\text{output}}$ and $\tilde{C}_{D\,\text{output}}$ into account. However, these coefficients were not calculated *a priori.* They had to be estimated from experiments for each system under consideration. On the contrary, in the present model, closure laws have been proposed for all the regular and singular loss coefficients involved. This makes this model entirely predictive, without requiring any complementary experimental input.

8. EXPERIMENTAL VALIDATION

The experimental validation presented in the following sections is based upon tests performed by de Langre *et al.* (1994).

8.1. Experimental Set-up

The experimental apparatus is schematically represented in Figure 5 and is described in detail by de Langre *et al.* (1994). Its main features are briefly reviewed hereafter.

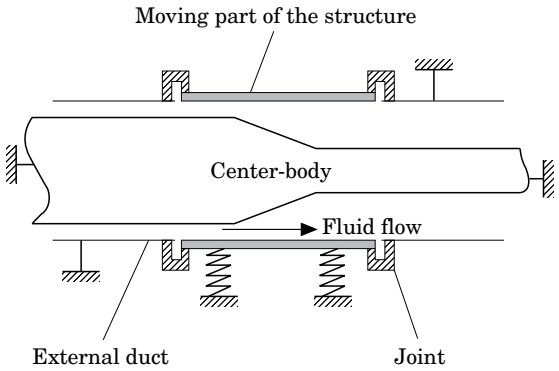

Figure 5. Schematic diagram of the experimental set-up.

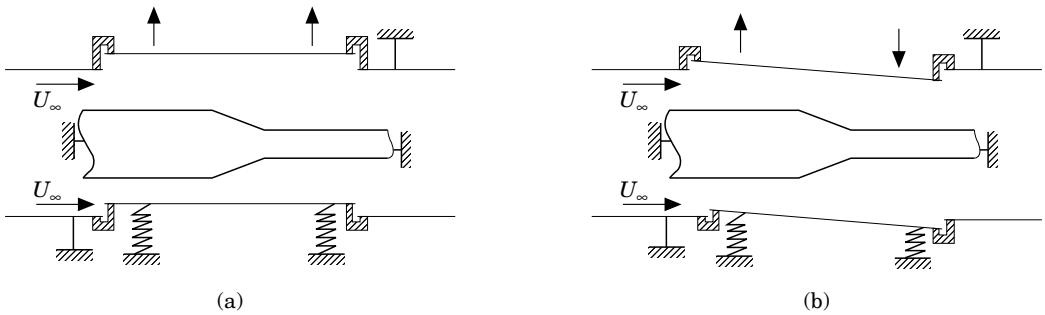

Figure 6. External duct: (a) translational and (b) rotational modes.

The experimental set-up consists of an axisymmetrical centre-body of variable section confined within a co-axial duct of constant diameter. The centre-body is composed of two cylinders connected with a 20° cone, the cylinder of larger section forming the upstream end of the centre-body. The centre-body is firmly fixed to the experimental set-up frame and is perfectly rigid. The external duct is rigid and fixed, except for its central part which is supported by two leaf-springs. This portion is free to oscillate in a plane, under the effect of an annular flow, according to a translational and a rotational mode of vibration (see Figure 6). The evolution versus flow rate of the resonance frequency and damping coefficient associated with each vibration mode of the coupled fluid–structure system is measured. The fluid used in this experiment is water.

8.2. Mechanical Modelling

The vibrating structure is supported by two leaf-springs of stiffness K_L, and by two joints characterized by their damping, C, and their stiffness, K. Denoting by M the physical mass of the moving structure, the vibrating system can be modeled as shown in Figure 7. As the moving structure is rigid, its motion can be expanded in terms of two normal modes,

$$w(z, t) = \phi_1(z)q_1(t) + \phi_2(z)q_2(t), \tag{38}$$

where the normal mode shapes, ϕ_1 and ϕ_2, are respectively defined by $\phi_1(z) = 1$, for the translational mode and $\phi_2(z) = z/L$ for the rotational mode (see Figure 6). The

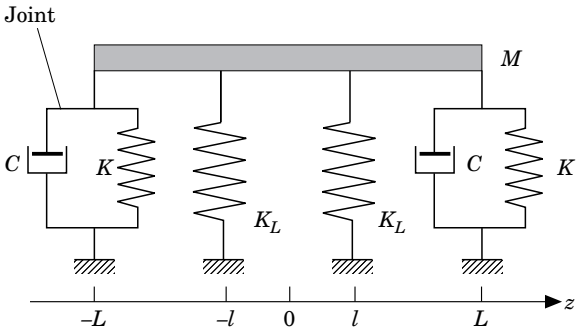

Figure 7. Mechanical model of the vibrating system.

equation of motion can thus be written in terms of the generalized coordinates (Thomson 1965). This yields

$$\begin{aligned} M\ddot{q}_1 + 2C\dot{q}_1 + 2(K + K_L)q_1 = 0, \\ \tfrac{1}{3}M\ddot{q}_2 + 2C\dot{q}_2 + 2[K + (l/L)^2 K_L]q_2 = 0. \end{aligned} \tag{39}$$

The values of M, C, K, and K_L measured by de Langre *et al.* (1994) can then be used to estimate from equation (39) the modal characteristics of the structure in still air.

8.3. Singular Loss Coefficient Modelling

In Section 5.2 we introduced two steady singular loss coefficients, $\bar{C}_{D\,\mathrm{input}}$, $\bar{C}_{D\,\mathrm{output}}$, and two unsteady singular loss coefficients, $\tilde{C}_{D\,\mathrm{input}}$, $\tilde{C}_{D\,\mathrm{output}}$, into the inlet-outlet boundary conditions. For the geometry under consideration, the values of the steady singular loss coefficients are obviously equal to zero, as there is no singularity at the inlet or outlet of the annular region when the movable part of the duct is at rest (Figure 5). However, geometric singularities are induced by structural motion, as shown in Figure 6. The values of the unsteady singular loss coefficients cannot therefore be equal to zero. They are estimated from a quasi-steady development of the steady laws for expansions and contractions.

Firstly, consider the joint at the inlet of the moving part of the duct. Let the duct oscillate with a harmonic motion, $\tilde{h}(\theta, 0, t)$, of circular frequency, ω, and amplitude h_o^+:

$$\tilde{h}(\theta, 0, t) = h_o^+ \cos(\theta)\cos(\omega t). \tag{40}$$

The motion-induced variation of the geometry near the joint is shown in Figure 8. Let $d\Gamma^-$ be the surface element represented in Figure 3 and located at θ on the exit cross-section of the *fixed* annular passage *upstream* of the joint; $d\Gamma^+(\theta, t)$ is a similar surface element located at θ on the entrance cross-section of the *time-varying* annular passage *downstream* of the joint. When the fluid flows from $d\Gamma^-$ to $d\Gamma^+(\theta, t)$, the geometry variation acts either as an expansion or a contraction, depending on the sign of $\tilde{h}(\theta, 0, t)$. A pressure variation, $\Delta p(\theta, t)$, thus takes place. The associated loss or pressure recovery coefficient, $\tilde{C}_{D\,\mathrm{input}}(\theta, t)$, can be determined in a quasi-steady way by assuming that, at each time, t, we can apply the results established for steady flows in Idelchik (1986). Therefore, $\tilde{C}_{D\,\mathrm{input}}(\theta, t)$ can be written in the following form

$$\tilde{C}_{D\,\mathrm{input}}(\theta, t) = K(\theta, t) f(d\Gamma^+(\theta, t)/d\Gamma^-). \tag{41}$$

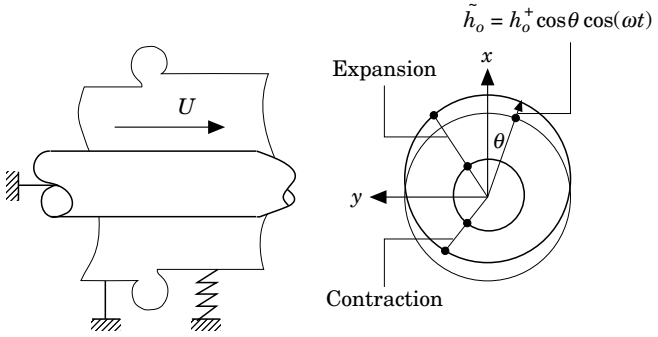

Figure 8. Variation of the geometry near the joints due to a harmonic motion of the duct.

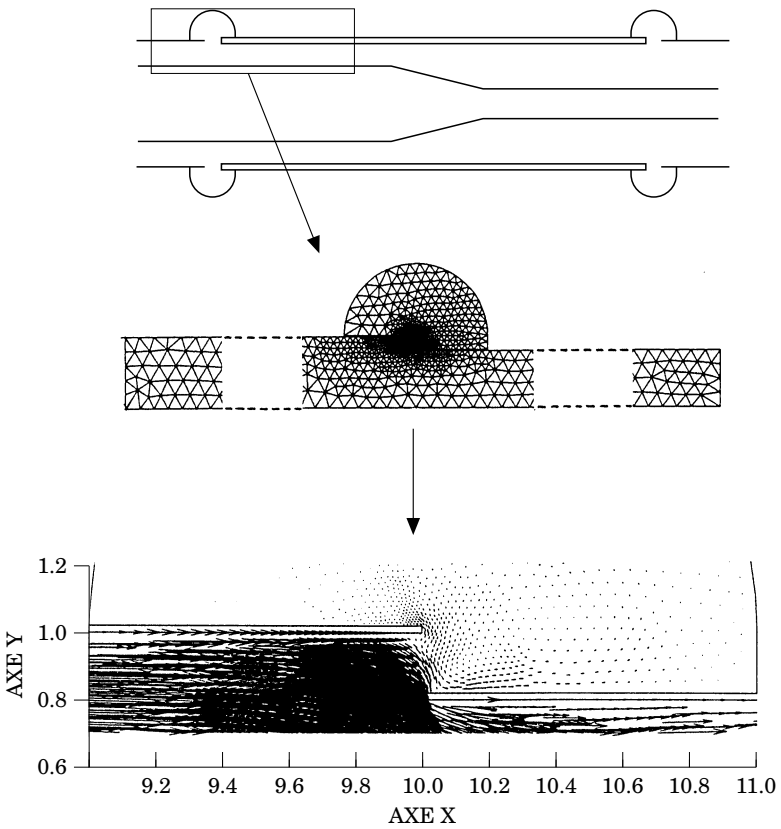

Figure 9. Unsteady singular loss coefficient modelling: a typical CFD result for a given static change in the position of the movable part of the duct.

(i) For $\tilde{h}(\theta, 0, t) \geq 0$, an expansion occurs. In this case, $K(\theta, t) = \text{const} \equiv K_e$ and

$$f(d\Gamma^+(\theta, t)/d\Gamma^-) \approx [1 - \bar{H}(0)/(\bar{H}(0) + \tilde{h}(\theta, 0, t))]^2 \approx 0, \tag{42}$$

at the second order.

(ii) For $\tilde{h}(\theta, 0, t) < 0$, a contraction occurs. In this case $K(\theta, t) = \text{const} \equiv K_r$ and

$$f(d\Gamma^+(\theta, t)/d\Gamma^-) \approx [1 - (\bar{H}(0) + \tilde{h}(\theta, 0, t))/\bar{H}(0)] \approx |\tilde{h}(\theta, 0, t)|/\bar{H}(0), \tag{43}$$

at second order.

This gives an expression for $\tilde{C}_{D\,\text{input}}$ which is a nonlinear function of $\tilde{h}(\theta, 0, t)$, and is periodic in θ and t. Within the framework of the small amplitude motion assumption, a linearized model has been derived from the first harmonic approximation of $\tilde{C}_{D\,\text{input}}(\theta, t)$. This yields

$$\tilde{C}_{D\,\text{input}} \approx K_r(h_o^+/\bar{H}(0))^{\frac{1}{2}} \cos(\theta) \cos(\omega t). \tag{44}$$

For an arbitrary motion, $\tilde{h}(\theta, 0, t)$, equation (44) can therefore be re-written as

$$\tilde{C}_{D\,\text{input}}(\theta, t) \approx \tfrac{1}{2}K_r[\tilde{h}(\theta, 0, t)/\bar{H}(0)]. \tag{45}$$

The unsteady singular coefficient $\tilde{C}_{D\,\text{output}}(\theta, t)$ can be determined in the same way. We obtain

$$\tilde{C}_{D\,\text{output}}(\theta, t) \approx \tfrac{1}{2}K_r[\tilde{h}(\theta, L, t)/\bar{H}(L)]. \tag{46}$$

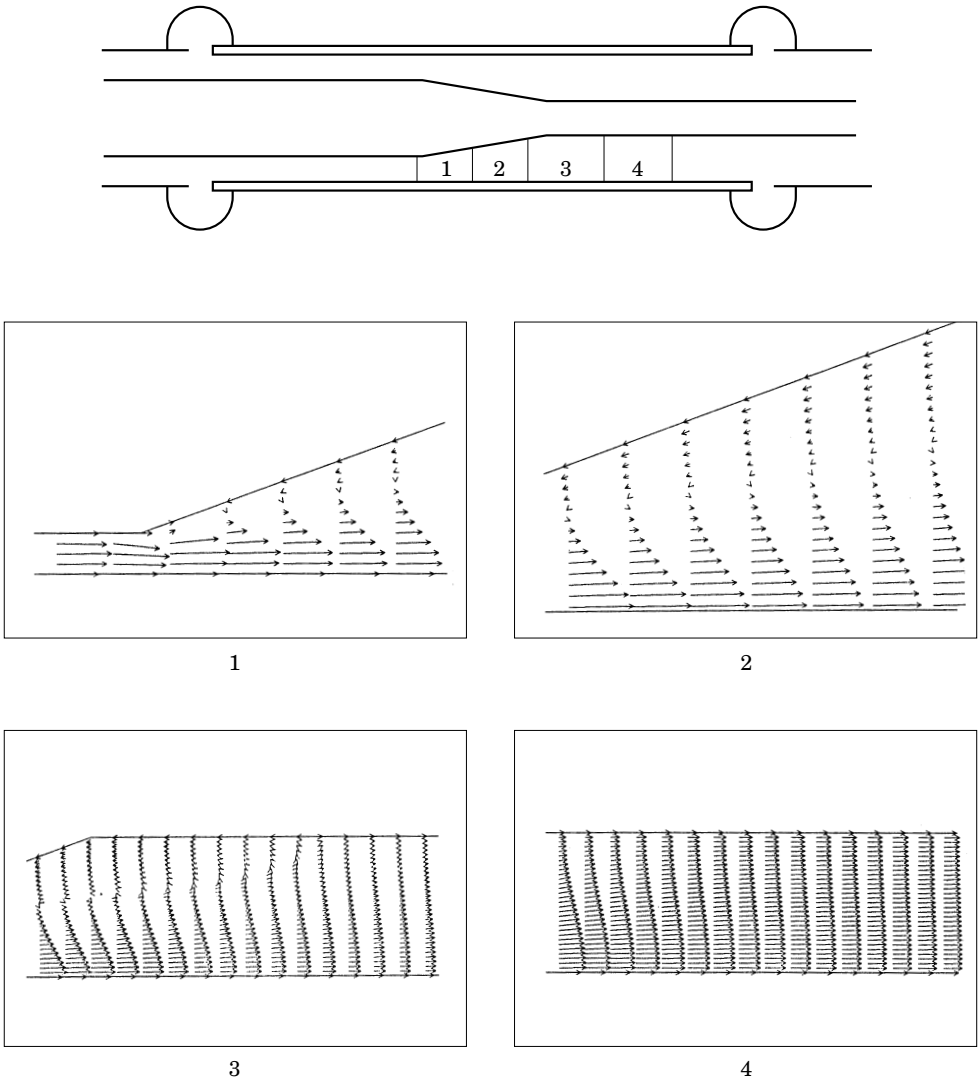

Figure 10. Computational result for the mean turbulent flow when the movable part of the duct is at rest.

Therefore, the quasi-steady interpretation of the results extablished in Idelchik (1986) allowed to specify the form of the analytical expressions for $\tilde{C}_{D\,\mathrm{input}}$ and $\tilde{C}_{D\,\mathrm{output}}$. However, the constant, K_r, which depends on the singularity involved, has still to be determined. This has been achieved from local pressure computation by using the CFD code N3S (Chabard 1992). A series of two-dimensional calculations has been performed for various *static* displacements of the movable duct. The local recirculations, induced at the entrance of the joint by a static change in the position of the movable part of the duct, are shown in Figure 9 which illustrates a typical steady flow computation performed to estimate the unsteady singular loss coefficients. A sensitivity analysis has been done by varying the incoming flow rate. We thus verified that K_r was approximately constant with a mean value of 2·1 and a standard derivation of 0·2.

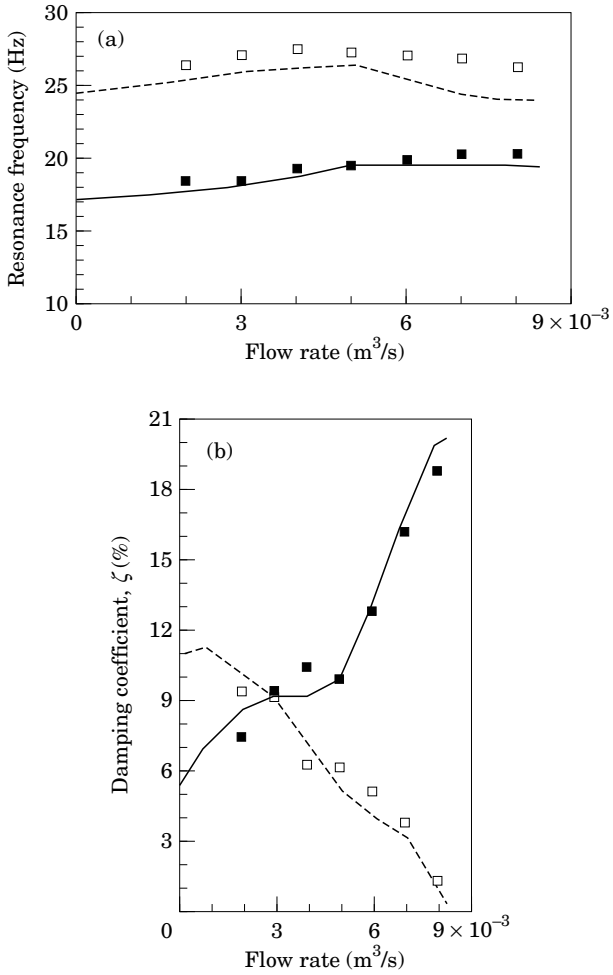

Figure 11. Comparison of the MOCCA results with experimental data. Variation of (a) resonance frequency and (b) damping coefficient versus flow rate. *Translational mode*: ■, experimental data; ——, MOCCA solution. *Rotational mode*: □, experimental data; - - - , MOCCA solution.

In this section, singular loss coefficient modelling has been presented for a specific geometry, in order to clarify the underlying ideas. However, the foregoing development shows that the method is quite general.

8.4. Comparison of the Experimental and Theoretical Results

For the system shown in Figure 5, the mean turbulent flow when the movable duct is at rest has first been calculated by the CFD code N3S (see Figure 10). Then, starting from the mechanical model determined in Section 8.2 and taking into account the mean turbulent flow, the parameters characterizing flow–structure interaction have been computed by the MOCCA code for various upstream flow velocities.

The results thus obtained can be compared to the experimental data of de Langre *et al.* (1994) in Figure 11. This figure shows the variation with flow rate of the resonance frequency and damping ratio for both modes of vibration. The agreement between the

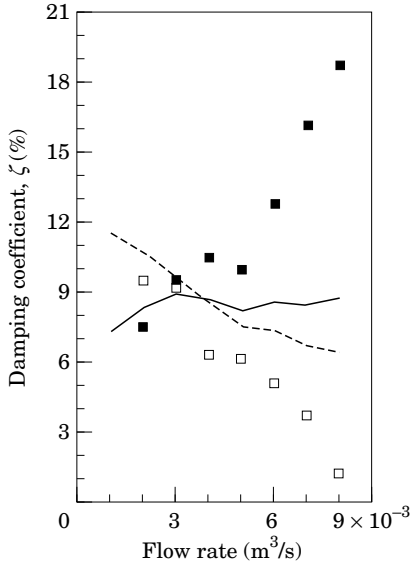

Figure 12. Comparison of Hobson's model with experimental data. Variation of the damping coefficient versus flow rate. *Translational mode*: ■, experimental data; ——, Hobson's model results. *Rotational mode*: □, experimental data; - - -, Hobson's model results.

MOCCA results and the experimental data is very good. In particular, according to the numerical solution, the translational mode is stable and the rotational mode becomes unstable for a flow rate of $8{\cdot}4 \times 10^{-3}\,m^3/s$. This closely reproduces the experimental observation.

The same configuration has also been calculated using Hobson's model (1982). The values of the regular and inlet–outlet singular loss coefficients were obtained from the closure laws of the MOCCA formulation. They were thus identical to those used in the MOCCA computation. The centre-body was modelled by two cylinders with constant radii, equal to those of the upstream and downstream cylinders, respectively. The inter-element compatibility condition took into account a pressure coefficient corresponding to a 20° diffuser derived from Idelchik (1986). The damping variation with flow rate calculated with Hobson's model can be compared to experimental data in Figure 12. Although the qualitative agreement may be considered as satisfactory, quantitative accord is not achieved. In particular Hobson's model does not predict any fluidelastic instability in this range of flow rates.

9. CONCLUSIONS

A model for simulating fluidelastic coupling between an oscillating cylindrical structure and an axial annular flow has been presented. It has been shown that this model can be considered as a generalization of Hobson's model. In its present form, it can deal with an incompressible viscous fluid, flowing at high Reynolds number, in a finite length annular region whose cross-section may vary continuously with axial position. It is implemented into the MOCCA code. An important point is that, although this model deals with turbulent flows and uses nonclassical boundary conditions, it is entirely predictive in the sense that it does not contain any adjustable parameter whose choice has to be guided by experimental results.

A first validation of this model was carried out in a previous paper (Perotin &

Granger 1992) using experimental data published by Mateescu *et al.* (1988). These experiments concerned a cylinder subjected to a flow in an annular region of *constant* cross-section and whose motion was imposed by a shaker. The numerical results obtained with the MOCCA code were in very good agreement with the experimental data. In this paper, the validation process has been carried on. This time, attention has been focused on time-varying annular passages of *variable* cross-section and on true *fluidelastic coupling.* The numerical results obtained with MOCCA have been compared to the solution of Hobson's model and to the experimental data of de Langre *et al.* (1994). In these experiments, the outer cylinder of an axially variable annulus was free to oscillate under the action of the flow. This comparison shows that the model presented in this paper is a clear improvement to Hobson's model, leading to a more reasonable agreement with experimental results.

References

Chabard, J. P. 1990 A finite element method for turbulent incompressible flows. Computational Fluid Dynamics for Industrial Flows Series, Von Karman Institute of Fluid Dynamics Lectures.

Dorodnitsyn, A. A. 1956 Solution of mathematical and logical problems on high-speed digital computers. *Proceedings Conference on Development of Soviet Machines and Devices,* Part 1, pp. 44–52. Moscow: VINITI.

Gunzburger, M. D. & Nicolaides, R. A. 1993 *Incompressible Computational Fluid Dynamics.* Cambridge: Cambridge University Press.

Hobson, D. E., 1982 Fluid elastic instabilities caused by flow in an annulus. *Proceedings of the BNES Third International Conference on Vibration of Nuclear Plant,* pp. 440–463. Keswick, U.K.

Holt, M. 1984 *Numerical Methods in Fluid Dynamics.* New York: Springer-Verlag.

Idelchik, I. E. 1986 *Handbook of Hydraulic Resistance.* New York: Hemisphere Publishing Corporation.

Inada, F. & Hayama, S., 1990 A study on leakage-flow-induced vibrations. Part 1: Fluid-dynamic forces and moments acting on the walls of a narrow tapered passage. *Journal of Fluids and Structures* **4,** 395–412.

de Langre, E., Belanger, F. & Porchet, G. 1992 Linearized potential flow theory applied to the calculation of fluidelastic forces in annular flow. *Proceedings of the 3rd International ASME Symposium on Flow-Induced Vibration and Noise,* Vol. **5,** (eds M. P. Païdoussis & M. K. Au Yang), pp. 187–204, Anahemim, CA. New York: ASME.

de Langre, E., Porchet, G. & Axisa, F. 1994 An experiment on fluidelastic instability in a confined annular flow. *Proceedings of the 2nd International Conference on Engineering Aero-Hydro Elasticity,* pp. 32–36. Pilsen., Czech Republic.

Mateescu, D. & Païdoussis, M. P. 1985 The unsteady potential flow in an axially variable annulus and its effect on the dynamics of the oscillating rigid center-body. *ASME Journal of Fluids Engineering* **107,** 421–427.

Mateescu, D. & Païdoussis, M. P. 1987 Unsteady viscous effect on the annular flow-induced instabilities of a rigid cylindrical body in a narrow duct. *Journal of Fluids and Structures* **1,** 197–215.

Mateescu, D., Païdoussis, M. P. & Belanger, F. 1988 Pressure measurements on an unsteady oscillating cylinder in a narrow annular flow. *Journal of Fluids and Structures* **2,** 615–628.

Mateescu, D., Païdoussis, M. P. & Belanger, F. 1994 Unsteady annular viscous flows between oscillating cylinders. Part 1: Computational solution based on a time-integration method. *Journal of Fluids and Structures* **8,** 489–507.

Mateescu, D., Pottier, T., Perotin, L. & Granger, S. 1995 Three-dimensional unsteady viscous flows between oscillating eccentric cylinders by an enhanced hybrid spectral method. *Journal of Fluids and Structures* **9,** 671–695.

Mulcahy, T. M. 1988 One-dimensional leakage-flow vibration instabilities. *Journal of Fluids and Structures* **2,** 383–403.

Perotin, L. & Granger, S. 1992 A numerical model for fluid-structure coupling of a confined

cylinder submitted to an axial annular flow. *Proceedings of the 3rd ASME International Symposium on Flow-Induced Vibration and Noise,* Vol. 5, (eds M. P. Païdoussis & M. K. Au Yang), pp. 1–16, Anaheim.

PRANDTL, L. 1936 *The Mechanics of Viscous Fluids,* Berlin: Springer Editions.

RICHARDSON, S. M. 1989 *Fluid Mechanics.* New York: Hemisphere Publishing Corporation.

SCHLICHTING, H., 1968 *Boundary Layer Theory.* New York: McGraw-Hill.

SPURR, A. & HOBSON, D. E. 1984 Forces on the vibrating centrebody of an annular diffuser. *Proceedings of the 1st ASME International Symposium on Flow-Induced Vibrations,* (eds M. P. Païdoussis & M. K. Au-Yang), pp. 41–52. New Orleans, LA. New York: ASME.

THOMSON, W. T. 1965 *Vibration Theory and Applications.* Englewood Cliffs, N.J.: Prentice Hall.

ZWILLINGER, D. 1989 *Handbook of Differential Equations.* San Diego: Academic Press, Inc.

APPENDIX A: LINEAR MOMENTUM CONSERVATION EQUATIONS ASSOCIATED WITH THE CONTINUITY EQUATION (16)

θ direction

$$\begin{aligned}
&\left[\frac{\bar H}{2}\int_{-1}^{+1}\left(\bar R_0+\eta\frac{\bar H}{2}\right)\phi_z\,\mathrm{d}\eta\right]\frac{\partial\tilde u_\theta^+}{\partial t}+\frac{\partial}{\partial z}\left[\frac{\bar H\bar U_z^+}{2}\int_{-1}^{+1}\left(\bar R_0+\eta\frac{\bar H}{2}\right)\phi_z^2\,\mathrm{d}\eta\right]\tilde u_\theta^+\\
&\quad+\left[\frac{\bar H\bar U_z^+}{2}\int_{-1}^{+1}\left(\bar R_0+\eta\frac{\bar H}{2}\right)\phi_z^2\,\mathrm{d}\eta\right]\frac{\partial\tilde u_\theta^+}{\partial z}+\left[\frac{\bar H\bar U_r^+}{2}\int_{-1}^{+1}\phi_r\phi_z\,\mathrm{d}\eta\right]\tilde u_\theta^+ +\frac{1}{\rho}\left[\frac{\bar H}{2}\int_{-1}^{+1}\phi_p\,\mathrm{d}\eta\right]\frac{\partial\tilde p^+}{\partial\theta}\\
&\quad+\frac{1}{\rho}\left[\frac{\bar P^+}{2}\int_{-1}^{+1}\phi_p\,\mathrm{d}\eta\right]\frac{\partial\tilde h}{\partial\theta}+\frac{\bar P^+}{\rho}\phi_p(-1)\frac{\partial\tilde r_1}{\partial\theta}-\frac{\bar P^+}{\rho}\phi_p(1)\frac{\partial\tilde r_2}{\partial\theta}\\
&=\frac{1}{\rho}(\bar r_2\bar\tau_\theta^*|_{\eta=1}+\bar r_1\bar\tau_\theta^*|_{\eta=-1}+\tilde r_2\bar\tau_\theta^*|_{\eta=1}+\tilde r_1\bar\tau_\theta^*|_{\eta=-1})+\frac{1}{\rho}\frac{\partial}{\partial\theta}\left[\frac{\tilde h}{2}\int_{-1}^{+1}\bar\tau_{\theta\theta}\,\mathrm{d}\eta\right]\\
&\quad+\frac{1}{\rho}\frac{\partial}{\partial\theta}\left[\frac{\bar H}{2}\int_{-1}^{+1}\tilde\tau_{\theta\theta}\,\mathrm{d}\eta\right]+\frac{1}{\rho}\frac{\tilde h}{2}\int_{-1}^{+1}\bar\tau_{r\theta}\,\mathrm{d}\eta\\
&\quad+\frac{1}{\rho}\frac{\partial}{\partial z}\left[\frac{\bar H}{2}\int_{-1}^{+1}\left(\bar R_0+\eta\frac{\bar H}{2}\right)\tilde\tau_{\theta z}\,\mathrm{d}\eta\right]+\frac{1}{\rho}\frac{\bar H}{2}\int_{-1}^{+1}\tilde\tau_{r\theta}\,\mathrm{d}\eta\\
&\quad+\frac{1}{\rho}\frac{\partial}{\partial z}\left[\int_{-1}^{+1}\left[\left(\bar R_0+\eta\frac{\bar H}{2}\right)\frac{\tilde h}{2}+\left(\tilde r_0+\eta\frac{\tilde h}{2}\right)\frac{\bar H}{2}\right]\bar\tau_{\theta z}\,\mathrm{d}\eta\right].
\end{aligned}\tag{A1}$$

z direction

$$\begin{aligned}
&\left[\frac{\bar H}{2}\int_{-1}^{+1}\left(\bar R_0+\eta\frac{\bar H}{2}\right)\phi_z\,\mathrm{d}\eta\right]\frac{\partial\tilde u_z^+}{\partial t}+\left[\frac{\bar H\bar U_z^+}{2}\int_{-1}^{+1}\phi_z^2\,\mathrm{d}\eta\right]\frac{\partial\tilde u_\theta^+}{\partial\theta}\\
&\quad+\left[\bar H\bar U_z^+\int_{-1}^{+1}\left(\bar R_0+\eta\frac{\bar H}{2}\right)\phi_z^2\,\mathrm{d}\eta\right]\frac{\partial\tilde u_z^+}{\partial z}+\left[\frac{\bar H}{2\rho}\int_{-1}^{+1}\left(\bar R_0+\eta\frac{\bar H}{2}\right)\phi_p\,\mathrm{d}\eta\right]\frac{\partial\tilde p^+}{\partial z}\\
&\quad+\frac{\partial}{\partial z}\left[\bar H\bar U_z^+\int_{-1}^{+1}\left(\bar R_0+\eta\frac{\bar H}{2}\right)\phi_z^2\,\mathrm{d}\eta\right]\tilde u_z^+ +\frac{1}{\rho}\phi_p(-1)\frac{\partial\bar r_1}{\partial z}\bar r_1\tilde p^+-\frac{1}{\rho}\phi_p(1)\frac{\partial\bar r_2}{\partial z}\bar r_2\tilde p^+\\
&\quad+\frac{1}{\rho}\frac{\partial}{\partial z}\left[\frac{\bar H}{2}\int_{-1}^{+1}\left(\bar R_0+\eta\frac{\bar H}{2}\right)\phi_p\,\mathrm{d}\eta\right]\tilde p^+\\
&\quad+\frac{1}{\rho}\frac{\partial}{\partial z}\left[\bar P^+\int_{-1}^{+1}\left[\left(\bar R_0+\eta\frac{\bar H}{2}\right)\frac{\tilde h}{2}+\left(\tilde r_0+\eta\frac{\tilde h}{2}\right)\frac{\bar H}{2}\right]\phi_p\,\mathrm{d}\eta\right]\\
&\quad+\frac{\partial}{\partial z}\left[\bar U_z^{+2}\int_{-1}^{+1}\left[\left(\bar R_0+\eta\frac{\bar H}{2}\right)\frac{\tilde h}{2}+\left(\tilde r_0+\eta\frac{\tilde h}{2}\right)\frac{\bar H}{2}\right]\phi_z^2\,\mathrm{d}\eta\right]
\end{aligned}$$

$$+\frac{1}{\rho}\bar{P}^{+}\left[\phi_p(-1)\left(\frac{\partial\bar{r}_1}{\partial z}\tilde{r}_1+\frac{\partial\tilde{r}_1}{\partial z}\bar{r}_1\right)-\phi_p(1)\left(\frac{\partial\bar{r}_2}{\partial z}\tilde{r}_2+\frac{\partial\tilde{r}_2}{\partial z}\bar{r}_2\right)\right]$$

$$+\left[\frac{\bar{U}_z^{+}}{2}\int_{-1}^{+1}\left(\bar{R}_0+\eta\frac{\bar{H}}{2}\right)\phi_z\,\mathrm{d}\eta\right]\frac{\partial\tilde{h}}{\partial t}+\frac{\bar{U}_z^{+}\bar{H}}{2}\frac{\partial}{\partial t}\left[\int_{-1}^{+1}\left(\tilde{r}_0+\eta\frac{\tilde{h}}{2}\right)\phi_z\,\mathrm{d}\eta\right]$$

$$=\frac{1}{\rho}(\tilde{r}_2\bar{\tau}_z^{*}|_{\eta=1}+\bar{r}_2\tilde{\tau}_z^{*}|_{\eta=1}+\tilde{r}_1\bar{\tau}_z^{*}|_{\eta=-1}+\bar{r}_1\tilde{\tau}_z^{*}|_{\eta=-1})$$

$$+\frac{\partial}{\partial\theta}\left[\frac{\bar{H}}{2\rho}\int_{-1}^{+1}\tilde{\tau}_{\theta z}\,\mathrm{d}\eta\right]+\frac{1}{\rho}\frac{\partial}{\partial\theta}\left[\frac{\tilde{h}}{2}\int_{-1}^{+1}\bar{\tau}_{\theta z}\,\mathrm{d}\eta\right]+\frac{1}{\rho}\frac{\partial}{\partial z}\left[\frac{\bar{H}}{2}\int_{-1}^{+1}\left(\bar{R}_0+\eta\frac{\bar{H}}{2}\right)\tilde{\tau}_{zz}\,\mathrm{d}\eta\right]$$

$$+\frac{1}{\rho}\frac{\partial}{\partial z}\left[\int_{-1}^{+1}\left[\left(\bar{R}_0+\eta\frac{\bar{H}}{2}\right)\frac{\tilde{h}}{2}+\left(\tilde{r}_0+\eta\frac{\tilde{h}}{2}\right)\frac{\bar{H}}{2}\right]\bar{\tau}_{zz}\,\mathrm{d}\eta\right]. \tag{A2}$$

APPENDIX B: VARIATIONS OF m and $\bar{C}_F$ WITH REYNOLDS NUMBER, INCLUDING ROUGHNESS EFFECTS

Let k being the wall roughness, D_H the hydraulic diameter, and Re_c the critical Reynolds number usually defined as Idelchik (1986) $\mathrm{Re}_c=(17{\cdot}85D_H/k)^{1{\cdot}143}$ The variations of m and $\bar{C}_F$ with Reynolds number are implemented into the MOCCA codes as follows:

(i) *for laminar flow* ($\mathrm{Re}\leq 2000$):

$$m=-1 \quad \text{and} \quad \bar{C}_F=16\,\overline{\mathrm{Re}}^{-1};$$

(ii) *for transitional flow* ($2000<\mathrm{Re}\leq 4000$):

$$m=0{\cdot}312 \text{ and } C_F=7.45\,10^{-4}\,\overline{\mathrm{Re}}^{0{\cdot}312};$$

(iii) *for hydraulically smooth turbulent flow* ($4000\leq\mathrm{Re}<\mathrm{Re}_c$):

$$\text{if } \mathrm{Re}\leq 10^5, \quad m=-0{\cdot}25 \text{ and } \bar{C}_F=0{\cdot}079\,\overline{\mathrm{Re}}^{-0{\cdot}25},$$

$$\text{if } \mathrm{Re}>10^5, \quad m=-\frac{0{\cdot}87}{\log(\overline{\mathrm{Re}})-0{\cdot}91} \quad \text{and} \quad \bar{C}_F=\frac{0{\cdot}25}{(1{\cdot}8\log(\overline{\mathrm{Re}})-1{\cdot}64)^2};$$

(iv) *for fully rough turbulent flow* ($\mathrm{Re}\geqq\mathrm{Re}_c$):

$$\text{if } \mathrm{Re}_c\leq 10^5, \quad m=0 \text{ and } \bar{C}_F=0{\cdot}079\,\mathrm{Re}_c^{-0{\cdot}25},$$

$$\text{if } \mathrm{Re}_c>10^5, \quad m=0 \text{ and } \bar{C}_F=\frac{0.25}{(1{\cdot}8\log(\mathrm{Re}_c)-1{\cdot}64)^2}.$$